

# RSC Advances



This is an *Accepted Manuscript*, which has been through the Royal Society of Chemistry peer review process and has been accepted for publication.

*Accepted Manuscripts* are published online shortly after acceptance, before technical editing, formatting and proof reading. Using this free service, authors can make their results available to the community, in citable form, before we publish the edited article. This *Accepted Manuscript* will be replaced by the edited, formatted and paginated article as soon as this is available.

You can find more information about *Accepted Manuscripts* in the [Information for Authors](#).

Please note that technical editing may introduce minor changes to the text and/or graphics, which may alter content. The journal's standard [Terms & Conditions](#) and the [Ethical guidelines](#) still apply. In no event shall the Royal Society of Chemistry be held responsible for any errors or omissions in this *Accepted Manuscript* or any consequences arising from the use of any information it contains.

1 **Tandem Catalytic Conversion of 1-Butene and Ethene to Propene over Combined**  
2 **Mesoporous W-FDU-12 and MgO Catalysts**

3 Wei Xu<sup>a,b</sup>, Chao Lin<sup>a</sup>, Huan Liu<sup>a</sup>, Hongbo Yu<sup>a</sup>, Kai Tao<sup>a\*</sup>, Shenghu Zhou<sup>a\*</sup>

4 <sup>a</sup>Ningbo Institute of Materials Technology and Engineering, Chinese Academy of Sciences,  
5 Ningbo, Zhejiang, 315201, P. R. China

6 <sup>b</sup>Center of Applied Solid State Chemistry Research, Ningbo University,  
7 Ningbo, Zhejiang, 315201, P. R. China

8

9

10

11

12

13

14

15

16

17

18

19

20 **\*Corresponding author**

21 Tel.: (+86) 574 86696927

22 Fax: (+86) 574 86685043

23 E-mail: zhoush@nimte.ac.cn, taokai@nimte.ac.cn

1 **Abstract** Tungsten substituted mesoporous FDU-12 (W-FDU-12) catalysts were synthesized  
2 by one-pot hydrothermal process using F127 as the structure directing agents. The studies of  
3 TEM, SAXS and BET illustrated that the highly ordered mesoporous structure of FDU-12  
4 was maintained in the doped W-FDU-12 samples. XPS studies revealed that high  
5 concentration of  $W^{5+}$  species appeared in doped W-FDU-12 catalysts whereas supported  
6  $WO_3/$ FDU-12 and  $WO_3/SiO_2$  catalysts only contained  $W^{6+}$  species. Tandem catalytic  
7 conversion of 1-butene and ethene to propene through isomerization of 1-butene to 2-butene  
8 and consecutive cross metathesis of 2-butene and ethene in a fixed-bed reactor at different  
9 temperatures and atmospheric pressure was used to evaluate the catalytic performance of  
10 W-FDU-12 catalyst, combined with MgO. The catalytic results showed that the doped  
11 W-FDU-12 illustrated a superior catalytic performance relative to the supported  $WO_3/$ FDU-12  
12 and  $WO_3/SiO_2$  catalysts. The higher metathesis activity of W-FDU-12 catalysts can be  
13 ascribed to the well dispersion of W species and the incorporation of W species into the  
14 framework of FDU-12, forming substantial amount of  $W^{5+}$ , which was beneficial for the cross  
15 metathesis of 2-butene and ethene to propene.

16 **Key Words:** FDU-12; metathesis; tungsten catalysts; propene

## 17 1. Introduction

18 Recently, there has been a continuously increasing demand of propene owing to the  
19 strong demand for polypropene. Several production technologies including propane  
20 dehydrogenation,<sup>1,2</sup> catalytic cracking of  $C_4^+$  olefin<sup>3,4</sup> and methanol to olefin process,<sup>5</sup> are  
21 developed for propene production. Another effective pathway for propene production is the  
22 catalytic cross metathesis reaction of 1-butene (or 2-butene) and ethene.<sup>6-8</sup> The most  
23 important metathesis catalysts for propene production are those supported rhenium,  
24 molybdenum and tungsten oxides.<sup>9-13</sup> Among them, the  $WO_3/SiO_2$  catalysts are of special

1 interest due to lower price and good persistence. The metathesis of butene and ethene to  
2 propene using  $\text{WO}_3/\text{SiO}_2$  catalysts has been commercialized as the olefin conversion  
3 technology (OCT).<sup>14,15</sup>

4 The activity and selectivity of olefin metathesis over the supported tungsten oxide are  
5 dependent on the physicochemical properties of the supports, tungsten contents, pretreatment  
6 conditions and the oxidation states of tungsten species.<sup>16-19</sup> A variety of materials have been  
7 chosen as supports for W-containing catalyst, such as  $\text{SiO}_2$ ,  $\text{Al}_2\text{O}_3$ ,  $\text{TiO}_2$ , and mixed oxides  
8 including  $\text{SiO}_2\text{-Al}_2\text{O}_3$ ,  $\text{SiO}_2\text{-TiO}_2$ , and so on.<sup>20-23</sup> Mazoyer *et al.*<sup>24</sup> prepared W-H/ $\text{Al}_2\text{O}_3$   
9 catalysts for metathesis reaction of 2-butene and ethene, and the catalytic results showed that  
10 the W-H/ $\text{Al}_2\text{O}_3$  catalysts were stable and highly selective to propene formation even at  
11 substoichiometric ratios of ethene/2-butene. Hua *et al.*<sup>25</sup> synthesized the titanium-silica  
12 molecular sieve supported tungsten oxides for metathesis of butene to propene and pentene.  
13 The reported  $\text{WO}_3/\text{MTS-9}$  exhibited excellent catalytic performance, and the tetrahedral and  
14 the octahedral polytungsten species were speculated as active sites. These results have  
15 illustrated that different types of supports have significant effect on the catalytic performance  
16 of the W-containing catalysts.

17 Compared with the traditional supports, mesoporous silica materials show uniform pores,  
18 high BET surface areas, large pore volumes, and narrow pore size distribution, which is  
19 beneficial for dispersion of active species and provides rapid transportation channels for  
20 reactants and products. Several W doped mesoporous silica materials have been prepared for  
21 metathesis reactions.<sup>26-29</sup> Bhuiyan *et al.*<sup>27</sup> investigated the catalytic performance of W-SBA-15  
22 and W-MCM-41 catalysts for metathesis of 2-butene to propene, and found that these

1 materials exhibited the higher activity as compared to supported tungsten oxide catalysts.  
2 Moreover, W-MCM-41 materials were superior to W-SBA-15 at low reaction temperature  
3 because that W-MCM-41 had more number of tetrahedrally coordinated tungsten oxide  
4 species. Ramanathan *et al.*<sup>28</sup> prepared the W-KIT-5 by one-step direct hydrothermal synthesis  
5 procedure, and the catalysts show high dispersion of W species with the strong interaction  
6 between W species and KIT-5 silicate as evidenced by the co-existence of W<sup>5+</sup> and W<sup>6+</sup>  
7 species on the support surface. In our previous work,<sup>29</sup> we found that doped W-KIT-6  
8 exhibited much higher catalytic performance than traditional SiO<sub>2</sub> supported WO<sub>3</sub> catalysts in  
9 metathesis of 1-butene and ethene to propene.

10 Herein, we first reported W doped mesoporous materials (W-FDU-12) by one-pot  
11 synthesis method. The W-FDU-12 combined with MgO was applied in tandem catalytic  
12 conversion of 1-butene and ethene to propene. The schematic demonstration of this study was  
13 shown in Scheme 1. FDU-12 is a highly ordered large cage-type (12 to 60 nm) mesoporous  
14 silica with a cubic  $Fm\bar{3}m$  close-packed structure, allowing good accessibility for guest  
15 molecules.<sup>30–33</sup> In this study, the supported WO<sub>3</sub>/FDU-12 and WO<sub>3</sub>/SiO<sub>2</sub> catalysts with  
16 traditional impregnation method were also synthesized for comparison. Among these  
17 materials, the doped W-FDU-12 catalysts exhibited a superior catalytic performance for  
18 catalytic conversion of 1-butene and ethene relative to the supported WO<sub>3</sub>/FDU-12 and  
19 WO<sub>3</sub>/SiO<sub>2</sub> catalysts. The results revealed that the catalytic activity and selectivity were  
20 strongly dependent on the preparation method of catalysts, and the superior catalytic  
21 performance of W-FDU-12 originated from highly dispersed W species and high  
22 concentration of W<sup>5+</sup> species due to the doping method.

## 1    **2. Experimental**

### 2    **2.1. Chemicals.**

3        Triblock poly(ethylene oxide)-poly(propylene oxide)-poly(ethylene oxide) co-polymer  
4    Pluronic F127 ( $M_{av} = 12,600$ ,  $EO_{106}PO_{70}EO_{106}$ ) was purchased from Sigma-Aldrich.  
5    Tetraethyl orthosilicate (TEOS, 98%) and 1,3,5-trimethylbenzene (TMB, 97%) and MgO  
6    powders (99.9%) were purchased from Aladdin. Ammonium metatungstate  
7     $((NH_4)_6H_2W_{12}O_{40} \cdot xH_2O)$  was purchased from Kunshan Xingbang W&M Technology  
8    Company. Sodium tungstate dihydrate ( $Na_2WO_4 \cdot 2H_2O$ ), potassium chloride (KCl) and  
9    hydrochloric acid (HCl) were purchased from Shanghai Chemical Reagent Company. Silica  
10   gel (surface area  $399 \text{ m}^2/\text{g}$ ) was obtained from Qingdao Haiyang Chemical Co. Ltd.. All  
11   chemicals were used as received without further purification.

### 12   **2.2. Catalyst Preparation.**

#### 13   *2.2.1 Preparation of FDU-12.*

14        Pluronic F127 (2.00 g), TMB (5.00 g) and KCl (5.00 g) were dissolved in 120 mL of  
15    2 M HCl aqueous solution. The resultant mixture was stirred at  $15 \text{ }^\circ\text{C}$  for 1.0 hour. TEOS  
16    (8.32 g) was then dropwise added to the above solution with continuous stirring at  $15 \text{ }^\circ\text{C}$  for  
17    another 24 hours. The resulting mixture was transferred into a Telfon-lined autoclave and  
18    aged at  $100 \text{ }^\circ\text{C}$  for 24 hours. After cooling to room temperature, the solid was isolated by  
19    filtering, washing with water, and drying at  $70 \text{ }^\circ\text{C}$  in an oven. Finally, the dried material was  
20    then calcined in a muffle oven at  $550 \text{ }^\circ\text{C}$  for 4 hours with a ramping rate of  $1 \text{ }^\circ\text{C}/\text{min}$  to  
21    remove F127 surfactants to obtain FDU-12.

#### 22   *2.2.2 Preparation of W-FDU-12.*

1 Pluronic F127 (2.00 g), TMB (5.00 g) and KCl (5.00 g) were dissolved in 120 mL of  
2 2 M HCl aqueous solution. The resultant mixture was stirred at 15 °C for 1.0 hour.  
3 Appropriate amount of sodium tungstate dihydrate dissolved in 10 mL deionized water was  
4 then added into the above mixture. The resulting solution was further stirred for 0.5 hours,  
5 followed by dropwise addition of 8.32 g of TEOS. The obtained mixture was vigorously  
6 stirred at 15 °C for 24 hours, and was then transferred to a Teflon-lined autoclave, followed  
7 by heating at 100 °C for another 24 hours. After cooling to room temperature, the yellow  
8 powdery products were collected, washed, and calcined by the same procedure of FDU-12.  
9 Five catalysts with W contents of 1.2, 2.2, 3.0, 4.0, and 5.2% (determined by inductively  
10 coupled plasma (ICP)) were prepared, and denoted as W-FDU-12-1.2%, W-FDU-12-2.2%,  
11 W-FDU-12-3.0%, W-FDU-12-4.0% and W-FDU-12-5.2%, respectively. The effect of  
12 calcination temperatures was also investigated using the W-FDU-12 with the W content of 4.0  
13 wt %, and the materials obtained at calcination temperatures of 600, 650 and 700 °C were  
14 denoted as W-FDU-4.0%-600(cal), W-FDU-4.0%-650(cal) and W-FDU-4.0%-700(cal),  
15 respectively.

### 16 *2.2.3 Preparation of supported WO<sub>3</sub>/FDU-12 and WO<sub>3</sub>/SiO<sub>2</sub>.*

17 The supported WO<sub>3</sub>/FDU-12 and WO<sub>3</sub>/SiO<sub>2</sub> catalysts were prepared by impregnating 2.0  
18 g of the support powders with the aqueous solution containing required amount of ammonium  
19 metatungstate in 5 mL deionized water. After drying in an oven at 100 °C overnight, the  
20 powders were calcined by the same procedure of FDU-12. The catalysts were denoted as  
21 WO<sub>3</sub>/FDU-12-4.0% and WO<sub>3</sub>/SiO<sub>2</sub>-4.0%, where the real loadings of W were 4.0 wt %.

### 22 **2.3 Catalyst Characterization.**

1 X-ray diffraction (XRD) measurements were performed on a Bruker D8 Advance X-ray  
2 diffractometer using Cu  $K_{\alpha}$  radiation in the  $2\theta$  range of  $5^{\circ}$  to  $80^{\circ}$ . The average  $\text{WO}_3$  crystalline  
3 sizes were calculated using the half-width at half-height of the most intense peak of the  
4 diffraction pattern and the Scherrer equation. Small-angle X-ray scattering (SAXS) patterns  
5 were recorded using a Bruker Nanostar U small-angle X-ray scattering instrument with a  
6 rotating anode X-ray source and a Vantec-2000 two-dimensional detector. Inductively  
7 coupled plasma (ICP-OES) analysis was achieved to obtain the real W loading using  
8 Perkin-Elmer OPTIMA 2100 DV optical emission spectroscopy spectrometer. Transmission  
9 electron microscopy (TEM) observations were carried out on a JEOL 2100 transmission  
10 electron microscope operated at 200 kV. The oxide state of W species were studied by X-ray  
11 photoelectron spectroscopy (XPS) using an AXIS ULTRA DLD multifunctional X-ray  
12 photoelectron spectroscopy with an Al source. The data processing was performed with  
13 CaseXPS software. The infrared (IR) spectra were recorded from  $4000\text{--}400\text{ cm}^{-1}$  using a  
14 Bruker Tensor 27 spectrometer.

15  $\text{N}_2$  physical adsorption experiments were carried out on a Micrometrics ASAP-2020 M  
16 adsorption apparatus. The pore size distributions were obtained by Barrett-Joyner-Halenda  
17 (BJH) method. Before the tests, all the samples were degassed under vacuum at  $200\text{ }^{\circ}\text{C}$  for 5  
18 hours. Carbon deposition of spent catalysts was measured by a Seiko thermal gravimetric  
19 (TG/DTA) 6300 apparatus. The sample was heated from  $100$  to  $900\text{ }^{\circ}\text{C}$  at a heating rate of  
20  $10\text{ }^{\circ}\text{C}/\text{min}$  in an air atmosphere with a gas flow rate of  $200\text{ mL}/\text{min}$ .

## 21 **2.4 Catalytic study.**

22 Tandem catalytic conversion of 1-butene and ethene to propene was performed in a fixed-bed

1 reactor (i.d. 10 mm). In a typical test, 1.0 g of catalyst with the size of 20-40 mesh supported  
2 by an layer of inert SiO<sub>2</sub> beads were placed in the center of the reactor, and 1.2 g MgO with  
3 the size of 20-40 mesh were put on the top of the W-contained catalyst layer for the  
4 isomerization of 1-butene to 2-butene. An additional layer of inert SiO<sub>2</sub> beads covered the  
5 layer of MgO. Before catalytic tests, the catalysts were activated *in situ* at 550 °C for 4 hours  
6 in a pure N<sub>2</sub> stream with a flow rate of 35 mL/min at 0.1 MPa to remove the moisture. After  
7 the reactor cooling down to reaction temperatures, ethene and 1-butene were then fed into the  
8 system. The catalytic reaction was carried out at the conditions of 400-500 °C, 0.1 MPa,  
9 weight hourly space velocity (WHSV, 1-C<sub>4</sub>H<sub>8</sub>+C<sub>2</sub>H<sub>4</sub>) of 0.9 h<sup>-1</sup> and a 1-butene/ethene molar  
10 ratio of 1/2. The products were analyzed by an online gas chromatograph (GC) equipped with  
11 a flame ionization detector (FID). The 1-butene conversion and propene selectivity were  
12 calculated according to the literatures,<sup>29,34</sup> as following:

$$13 \quad C_{1-butene} = \frac{[C_3]_n / 2 + [2-C_4]_n}{[C_3]_n / 2 + [1-C_4]_n + [2-C_4]_n} \quad (1)$$

$$14 \quad S_{propene} = \frac{[C_3]_m}{[C_3]_m + [2-C_4]_m} \quad (2)$$

15 Where [C<sub>3</sub>]<sub>n</sub>, [1-C<sub>4</sub>]<sub>n</sub> and [2-C<sub>4</sub>]<sub>n</sub> were the molar fraction of propene, 1-butene and 2-butene in  
16 effluent gases, respectively. And [C<sub>3</sub>]<sub>m</sub>, [1-C<sub>4</sub>]<sub>m</sub> and [2-C<sub>4</sub>]<sub>m</sub> were the weight percent of  
17 propene, 1-butene and 2-butene in effluent gases, respectively.

18

### 19 3. Results and Discussion

20 TEM images of various samples were displayed in Figure 1. As seen in Figure 1a, it  
21 clearly showed that this sample had typical FDU-12 cage-like mesostructures. The ordered

1 lattice array over large domains under the TEM observations suggested a uniform, cubic  
2 mesostructure ( $Fm\bar{3}m$ ) without intergrowth.<sup>35</sup> The diameter of the cages could be directly  
3 measured from the thin edge of the particle and was about 17.5 nm, in good accordance with  
4 the N<sub>2</sub> adsorption results (see below). As shown in Figure 1b-1d, the well-ordered  
5 mesoporous structures were observed in all W-FDU-12 materials. For lower W loading (1.2%,  
6 3.0% and 4.0%) doped catalysts, individual WO<sub>3</sub> particles cannot be found due to the  
7 incorporation of W species into framework. However, for high W loading catalyst  
8 W-FDU-12-5.2%, bulk WO<sub>3</sub> aggregations were observed in Figure 1e. However, the  
9 well-ordered mesoporous structure partially disappeared in Figure 1f for  
10 W-FDU-4.0%-700(cal), suggesting the collapse of the structure at high calcination  
11 temperature. For comparison, TEM images of FDU-12 supported WO<sub>3</sub>/FDU-12-4.0% catalyst  
12 and traditional silica supported WO<sub>3</sub>/SiO<sub>2</sub>-4.0% catalyst were present in Figure 1g and Figure  
13 1h. For the WO<sub>3</sub>/FDU-12-4.0% catalyst, it also exhibited the well-ordered array. But,  
14 nanosized WO<sub>3</sub> particles confined in the channels of FDU-12 with some particles present on  
15 the outer surfaces were observed. For the WO<sub>3</sub>/SiO<sub>2</sub>-4.0% catalyst, it clearly showed the WO<sub>3</sub>  
16 was dispersed on the surface of SiO<sub>2</sub> support as large agglomerates.

17 In order to investigate the oxidation states of W species in W-containing catalysts, XPS  
18 experiments were carried out. Figure 2 showed XPS spectra of W-FDU-12-4.0%,  
19 WO<sub>3</sub>/FDU-12-4.0%, WO<sub>3</sub>/SiO<sub>2</sub>-4.0% and W-FDU-12-4.0%-700(cal). The tungsten oxide  
20 species in different chemical states from the position of the W<sub>4f</sub> level was fitted by the  
21 curve-fitting procedure according to the theory of Doniach and Sunjic.<sup>36</sup> The intensity ratio  
22 between the W4f<sub>7/2</sub> and W4f<sub>5/2</sub> was fixed to 4/3, according to fitting rules.<sup>37</sup> Detailed

1 quantitative results from the peak-fitting results of  $W_{4f}$  were given in Table 1. As shown in  
2 Figure 2a, the doped W-FDU-12-4.0% catalyst contained two W species. The binding  
3 energies of 37.1 eV/35.0 eV and 38.4 eV/36.3 eV were attributed to the binding energies of  
4  $4f_{5/2}/4f_{7/2}$  of  $W^{5+}$  and  $W^{6+}$ , respectively.<sup>38</sup> The  $W^{5+}/W^{6+}$  ratio was 80.9/19.1 (4.24). XPS  
5 spectra of W-FDU-12 with various W loadings were also measured and the results were  
6 present in Figure S1 and Table S1. All the W-FDU-12 catalysts showed similar spectra  
7 (Figure S1) and contained substantial amount of  $W^{5+}$  (Table S1). The XPS spectra of  
8 mesoporous FDU-12 supported  $WO_3$ /FDU-12-4.0% (Figure 2b) and traditional silica  
9 supported  $WO_3/SiO_2$ -4.0% (Figure 2c) samples with the same W content only exhibited the  
10 highest oxidation state of  $W^{6+}$ . According to the literatures,<sup>29,39</sup> there were 5 kinds of structure  
11 of the tungsten oxide species in the W-doped SBA-15 and W-doped KIT-6 catalysts. Of them,  
12 three structures contained  $W^{5+}$  species.  $W^{5+}$  was induced by the strong interaction between W  
13 and Si through O bonding in the form of  $W = O - Si$  for doped W-SBA-15<sup>39</sup> and W-KIT-6.<sup>29</sup>  
14 In the present study, a high concentration of  $W^{5+}$  species in FDU-12 was possibly induced in a  
15 similar way. These  $W^{5+}$  species in catalysts may be beneficial to the catalytic performance for  
16 the metathesis of ethene and 1-butene to propene. In comparison, on the sample  
17 (W-FDU-12-4.0%-700(cal)) calcined at 700 °C, the  $W_{4f}$  peaks were also fitted with only one  
18  $W^{6+}$  doublet at 38.2 eV and 36.2 eV, as shown in Figure 2d, indicated that the W species were  
19 no longer doped into the framework due to the structure collapse, which was consistent with  
20 TEM observation in Figure 1f.

21 The  $N_2$  adsorption-desorption isotherms of FDU-12 and W-FDU-12 were shown in  
22 Figure 3 (left panel). For all the samples, they exhibited type IV isotherms with broad  $H_1$

1 hysteresis loops, which were typical for large-pore cage-like mesoporous silicas such as  
2 FDU-1, KIT-5, SBA-16 and so on.<sup>40-42</sup> The sharp capillary condensation feature at relative  
3 pressure of 0.45–0.90 ( $P/P_0$ ) indicated the existence of uniform pores in all samples. As  
4 discussed in the literatures, the delay of nitrogen capillary evaporation at 77 K to the lower  
5 pressure limit of hysteresis indicated that the diameters of the pore entrances to the cage-type  
6 pores in these mesostructural samples were smaller than 5 nm.<sup>43</sup> Table 2 summarized the BET  
7 surface areas, pore volumes and mean pore sizes of different samples. The BET surface area  
8 of FDU-12 was 717 m<sup>2</sup>/g. When W species was incorporated into the FDU-12 framework, the  
9 surface areas of these W-FDU-12 catalysts decreased slightly with increasing the tungsten  
10 loading, and reached 549 m<sup>2</sup>/g for the W-FDU-12-5.2% sample as shown in Table 2. The  
11 result confirmed that the doping method could maintain the textural properties of FDU-12 in  
12 the final W-FUD-12 catalysts.

13 The amount of W doped in catalysts affected the formation of the mesoporous matrix and  
14 its mesostructure differently. Figure 4 compared the SAXS spectra of the FDU-12  
15 mesoporous silica and W-contained catalysts, and all exhibited three main peaks, which could  
16 be indexed to the 111, 311, and 331 crystal lattices. These peaks reflected an ordered,  
17 face-centered cubic (fcc) structure (space group  $Fm\bar{3}m$ ).<sup>30-33</sup> From the SAXS results, there  
18 were no significant changes observed between FDU-12 and doped W-FDU-12,  
19 confirming the maintenance of long-range structural order either in FDU-12 support or in  
20 doped samples. It was also shown that the W-contained catalysts caused the shift of diffraction  
21 peaks to higher  $q$ -values in all spectra, indicating a reduction in cavity size for these doped  
22 materials.

1        The wide-angle X-ray diffraction patterns of FDU-12, doped W-FDU-12, WO<sub>3</sub>/FDU-12  
2        and WO<sub>3</sub>/SiO<sub>2</sub> samples were shown in Figure 5. It was observed that there was a broad  
3        diffraction in the  $2\theta$  range from 15° to 30° for all the samples, which was corresponding to the  
4        typical peak of an amorphous silica material. As shown in Figure 5b-5e, there were no  
5        obvious WO<sub>3</sub> diffractions for all catalysts, which indicated that basically all tungsten was  
6        highly dispersed or amorphous phase was formed. When increasing the W content to 5.2%  
7        wt%, crystalline WO<sub>3</sub> diffractions (PDF-83-0950) appeared as shown in Figure 5f, which was  
8        consistent with the TEM images in Figure 1e. Figure 5e, 5g and 5h showed the XRD profiles  
9        of W-FDU-12-4.0%, W/FDU-12-4.0% and W/SiO<sub>2</sub>-4.0% with the same W loading of 4.0  
10       wt%. No WO<sub>3</sub> diffractions were observed for W-FDU-12-4.0%. To confirm the presence of W  
11       species, EDX analysis was performed and the result was present in Figure S2. As shown in  
12       Figure S2, the signal of W was detected. Combined with XRD and TEM results it was  
13       suggested that the W was incorporated into the framework of FDU-12 for W-FDU-12-4.0%.  
14       The characteristic peaks at  $2\theta = 23.1^\circ$ ,  $23.6^\circ$ , and  $24.4^\circ$  corresponding to crystalline tungsten  
15       oxide (WO<sub>3</sub>, *P2<sub>1</sub>/n*) were observed for supported WO<sub>3</sub>/FDU-12-4.0% and WO<sub>3</sub>/SiO<sub>2</sub>-4.0%  
16       catalysts. The average WO<sub>3</sub> crystallines were 34 and 79 nm, respectively, suggesting that the  
17       crystallite size of FDU-12 based catalysts were smaller than that of conventional silica gel  
18       based catalysts. These XRD results revealed that the dispersion of W species decreased in the  
19       following sequence: doped W-FDU-12 > supported WO<sub>3</sub>/FDU-12 > supported WO<sub>3</sub>/SiO<sub>2</sub>,  
20       which was also confirmed by TEM observation.

21        The FTIR spectra of the FDU-12 and W-FDU-12 samples were shown in Figure 6. The  
22        characteristics absorption bands centered at 467, 799 and 1082 cm<sup>-1</sup> were attributed to the

1 bending modes of bulk Si–O–Si bond, symmetric and antisymmetric stretching vibration  
2 bands for the tetrahedral  $\text{SiO}_4^{4-}$  structure units. These vibrational bands were usually assigned  
3 as  $\delta(\text{Si–O–Si})$ ,  $\nu_s(\text{Si–O–Si})$  and  $\nu_{as}(\text{Si–O–Si})$  respectively, which accompanied by a  
4 progressive increase in intensity when tungsten content increased. The vibration at  $966\text{ cm}^{-1}$   
5 may be attributable to the W–O–Si linkage in the doped W-FDU-12 catalysts, indicating the  
6 successful incorporation of tungsten inside the silica framework.<sup>44</sup>

7 The W-contained catalysts were evaluated for catalytic conversion of 1-butene and ethene  
8 to propene. Because the metathesis reactions between olefins were reversible and competitive,  
9 a high ratio of ethene to 1-butene was favorable to the conversion of 1-butene into more  
10 propene. Industrial process used an ethene/butene ratio of 2/1 to obtain the best catalytic  
11 performance. Therefore, the comparison of different catalysts was carried out at the ratio of  
12 ethene/1-butene of 2/1. The careful analysis of products suggested that the main products of  
13 reaction over all of the W-FDU-12,  $\text{WO}_3/\text{FDU-12}$  and  $\text{WO}_3/\text{SiO}_2$  catalysts were propene and  
14 2-butene, only a little of byproduct (less than 0.2%) was found. Hence, the conversion of  
15 1-butene ( $C_{1\text{-butene}}$ ) and the selectivity of propene ( $S_{\text{propene}}$ ) were used to evaluate the  
16 performance of the different catalysts.

17 As discussed elsewhere, propene was mainly produced by the cross metathesis of 2-butene  
18 and ethene.<sup>14</sup> Therefore, the MgO was used as isomerization catalyst for conversion of  
19 1-butene to 2-butene during the reaction. The catalytic performance of single MgO or  
20 W-FDU-12-4% catalyst was present in Figure S3. As shown in Figure S3, only 32% 1-butene  
21 was converted and no propene was formed, indicating that the only role of MgO catalyst was  
22 isomerization of 1-butene to 2-butene. The 1-butene conversion (about 34%) and propene

1 selectivity (around 11%) were very low, when using single  $\text{WO}_x$ -containing catalyst. This  
2 suggested that the isomerization ability of W-FDU-12 was very poor due to neutral nature of  
3 FDU-12. In the present work, the reported catalytic performance was a combination of W  
4 contained catalysts and MgO. Since W contained catalysts were mixed with the same amount  
5 of MgO and the MgO had no contribution to metathesis (propene selectivity), the catalytic  
6 performances of W contained catalysts could be compared in this way.

7 To investigate the influence of the  $\text{WO}_3$  loading on catalyst activity, doped W-FDU-12  
8 catalysts containing 1.2, 2.2, 3.0, 4.0 and 5.2 wt% of W were prepared. Figure 7 showed the  
9  $C_{1\text{-butene}}$  and  $S_{\text{propene}}$  for the different W-containing catalysts at the reaction temperature of  
10 450 °C. The W-FDU-12 catalyst with lower W loading of 1.2% showed a poor catalytic  
11 performance. The 1-butene conversion and propene selectivity increased with increasing W  
12 loading. When the W content increased to 4.0%, the  $C_{1\text{-butene}}$  and  $S_{\text{propene}}$  reached a higher value  
13 with 78.8% and 89.9%, respectively. Further increasing the W loading, the catalytic  
14 performance exhibited slightly changes, although the molar fraction of  $\text{W}^{5+}$  species was less  
15 than that of  $\text{W}^{6+}$  (Table S1). However, the W loading was high and the absolute amount of  
16  $\text{W}^{5+}$  species was large. Therefore, the W-FDU-12-5.2% catalyst showed a high 1-butene  
17 conversion and propene selectivity. It should be noted that besides the metathesis, many  
18 side-reactions coexisted, such as, oligomerization<sup>27</sup> of ethene and/or butene to high molecular  
19 weight compound. At low W loading, the metathesis activity of butene and ethene to propene  
20 was low, and the oligomerization dominated. Therefore, the catalyst deactivated due to the  
21 formation of high molecular weight compound. To examine the effect of reaction temperature  
22 on the catalytic performance, W-FDU-12-4.0% catalyst at three different temperatures from

1 400, 450 and 500 °C was carried out and the results were shown in Figure S4. It could be seen  
2 that the activity of catalyst was affected greatly by reaction temperature. The 1-butene  
3 conversion and propene selectivity decreased with time on stream from 77.3% to 45.4% and  
4 89.8% to 49.8% at 400 °C, respectively. As discussed above, many side-reactions coexisted,  
5 such as oligomerization of ethene and/or butene to high molecular weight compound. At  
6 lower reaction temperature (400 °C), the metathesis active was low and the catalyst  
7 deactivated quickly due to the formation of high molecular weight compound. When the  
8 reaction temperature increased to 450 °C, the  $C_{1\text{-butene}}$  and  $S_{\text{propene}}$  increased slightly but with a  
9 good stability. Further increasing the temperature resulted in slightly improved catalytic  
10 performance.

11 According to previous results reported in literatures,<sup>45</sup> the calcination temperatures  
12 affected the nature of tungsten species of W-containing catalysts, which were active in the  
13 formation of propene by the metathesis reaction of ethene and butene. So the effect of  
14 calcination temperature on catalyst activity of W-FUD-12-4.0% was investigated in this study,  
15 and the results were shown in Figure S5. It can be seen that the calcination temperature from  
16 550 °C to 650 °C had no significant effect on  $C_{1\text{-butene}}$  and  $S_{\text{propene}}$ , which exhibited the similar  
17 catalytic performance. When the temperature increased to 700 °C, the W-FDU-4.0%-700(cal)  
18 sample showed poor catalytic activity due to the disappearance of  $W^{5+}$  species and the  
19 collapse of well-ordered mesoporous structure at high calcination temperature, which was  
20 also confirmed by the TEM observation in Figure 1f.

21 The catalytic performance of 4.0 wt% W-contained catalysts (W-FDU-12-4.0%,  
22  $WO_3$ /FDU-12-4.0% and  $WO_3$ /SiO<sub>2</sub>-4.0%) was present in Figure 8. The 1-butene conversion

1 and propene selectivity were decreased in the following sequence: doped W-FDU-12 >  
2 supported WO<sub>3</sub>/FDU-12 > supported WO<sub>3</sub>/SiO<sub>2</sub>, which was consistent with the catalytic  
3 performance of W-containing mesoporous KIT-6 for the metathesis of ethene and 1-butene to  
4 propene.<sup>29</sup> This phenomenon could be explained that the doping method could maintain the  
5 well-ordered mesoporous structure and effectively disperse W species with a high  
6 concentration of W<sup>5+</sup> species.

7 To investigate the carbon deposition of used catalysts, thermogravimetric analysis  
8 under air atmosphere was performed for the spent W-FDU-12-4.0%, WO<sub>3</sub>/FDU-12-4.0% and  
9 WO<sub>3</sub>/SiO<sub>2</sub>-4.0% catalysts after 8 h of reactions. Generally, the weight loss of used catalysts  
10 observed in TG study was due to removal of various types of carbon deposition. As shown in  
11 Figure S6, the total weight loss for the spent W-FDU-12-4.0%, WO<sub>3</sub>/FDU-12-4.0% and  
12 WO<sub>3</sub>/SiO<sub>2</sub>-4.0% samples were 2.7%, 4.4% and 8.0%, respectively. It was clearly suggested  
13 that the FDU-12 based catalysts had the lower carbon formation compared to the SiO<sub>2</sub>  
14 supported sample during catalytic reactions, and especially the doped W-FDU-12 had the  
15 lowest carbon deposition. The coke was caused by high molecular weight compound formed  
16 by side reactions. W-FDU-12 showed best metathesis activity and less side-reaction was  
17 occurred. Therefore, less coke was formed. TGA results showed the advantage of one-pot  
18 synthesized mesoporous W-FDU-12.

#### 19 **4. Conclusions**

20 This study first reported the using large-pore mesoporous silica FDU-12 to synthesize  
21 the doped W-FDU-12 catalysts (combined with MgO) for tandem catalytic conversion of  
22 1-butene and ethene to propene through isomerization of 1-butene to 2-butene and

1 consecutive cross metathesis of 2-butene and ethene, and compared with the supported  
2  $\text{WO}_3/\text{FDU-12}$  and  $\text{WO}_3/\text{SiO}_2$  catalysts. For doped W-FDU-12, tungsten was successfully  
3 incorporated into the framework of mesoporous silica. Cubic three-dimensional mesoporous  
4 structure with a high degree of long-range ordering was evident for all tungsten doped  
5 catalysts from SAXS, BET and TEM analysis. The XPS results illustrated that W species were  
6 incorporated into the FDU-12 framework with a high concentration  $\text{W}^{5+}$  species for  
7 W-FDU-12. The 1-butene conversion and propene selectivity of doped W-FDU-12 catalyst  
8 were much better than those of supported  $\text{WO}_3/\text{FDU-12}$  and  $\text{WO}_3/\text{SiO}_2$  catalysts. The doped  
9 W-FDU-12 with 4.0 wt% tungsten content exhibited a good catalytic performance with  
10 1-butene conversion and propene selectivity of 78.8% and 89.9%, respectively. The optimal  
11 calcination temperature and metathesis reaction temperature were 550 °C and 450 °C,  
12 respectively. These results suggested that W-FDU-12 materials had promising application as  
13 catalytic materials in tandem catalytic conversion of 1-butene and ethene to propene to  
14 product propene through metathesis, and could be extended to other olefin metathesis  
15 reactions.

## 16 Acknowledgments

17 K. Tao thanks the financial support from the National Natural Science Foundation of  
18 China (Grant No. 51302278). S. Zhou thanks the Ministry of Science and Technology of  
19 China (Grant No. 2012DFA40550) for financial supports.

## 20 References

- 21 1 J. Pless, B. Bardin, H. Kim, D. Ko, M. Smith, R. Hammond, P. Stair, K. Poepelmeier, *J.*  
22 *Catal.*, 2004, **223**,419–31.
- 23 2 L. Liu, Q. Deng, B. Agula, X. Zhao, T. Ren, Z. Yuan, *Chem. Commun.*, 2011, **47**,  
24 8334–8336.

- 1 3 O. Muraza, I. Bakare, T. Tago, K. Konno, T. Taniguchi, A. Al-Amer, Z. Yamani, Y.  
2 Nakasaka, T. Masuda, *Fuel*, 2014, **135**, 105–111.
- 3 4 G. Zhao, J. Teng, Z. Xie, W. Jin, W. Yang, Q. Chen, Y. Tang, *J. Catal.*, 2008, **248**, 29–37.
- 4 5 X. Wang, M. Wen, C. Wang, J. Ding, Y. Sun, Y. Liu, Y. Lu, *Chem. Commun.*, 2014, **50**,  
5 6343–6345.
- 6 6 Y. Chauvin, *Angew. Chem. Int. Ed.*, 2006, **45**, 3741–3747.
- 7 7 E. Mazoyer, K. Szeto, N. Merle, S. Nordic, O. Boyron, J. Basset, M. Taoufik, C. Nicholas, *J.*  
8 *Catal.*, 2013, **301**, 1–7.
- 9 8 T. Hahn, E. Kondratenko, D. Linke, *Chem. Commun.*, 2014, **50**, 9060–9063.
- 10 9 W. Limsangkass, S. Phatanasri, P. Praserttham, J. Panpranot, W. Jareewatchara, S. Ayudhya,  
11 K. Suriye, *Catal. Lett.*, 2013, **143**, 919–925.
- 12 10 D. Zhang, X. Li, S. Liu, S. Huang, X. Zhu, F. Chen, S. Xie, L. Xu, *Appl. Catal. A*, 2012,  
13 **439–440**, 171–178.
- 14 11 C. Lin, K. Tao, H. Yu, D. Hua, S. Zhou, *Catal. Sci. Technol.*, 2014, **4**, 4010–4019.
- 15 12 X. Solans-Monfort, E. Clot, C. Coperet, O. Eisenstein, *J. Am. Chem. Soc.*, 2005, **127**,  
16 14015–14025.
- 17 13 N. Poovarawan, K. Suriye, S. Ayudhya, J. Punpranot, F. Aires, P. Praserttham, *Catal. Lett.*,  
18 2014, **144**, 920–927.
- 19 14 J. C. Mol, *J. Mol. Catal. A*, 2004, **213**, 39–45.
- 20 15 A. Spamer, T. Dube, D. Moodley, C. Van Schalkwyk, J. Botha, *Appl. Catal. A*, 2003, **255**,  
21 133–142.
- 22 16 Z. Cheng, C. Lo, *ACS Catal.*, 2012, **2**, 341–349.
- 23 17 X. Yang, R. Gao, W. Dai, K. Fan, *J. Phys. Chem. C*, 2008, **112**, 3819–3826.
- 24 18 Y. Wang, Q. Chen, W. Yang, Z. Xie, W. Xu, D. Huang, *Appl. Catal. A*, 2003, **250**, 25–37.
- 25 19 S. Huang, F. Chen, S. Liu, Q. Zhu, X. Zhu, W. Xin, Z. Feng, C. Li, Q. Wang, L. Xu, *J. Mol.*  
26 *Catal. A*, 2007, **267**, 224–233.
- 27 20 A. Andreini, J. C. Mol, *J. Chem. Soc., Faraday Trans. 1*, 1985, **81**, 1705–1714.
- 28 21 D. Debecker, M. Stoyanova, U. Rodemerck, F. Colbeau-Justin, C. Boissère, A.  
29 Chaumonnot, A. Bonduelle, C. Sanchez, *Appl. Catal. A*, 2014, **470**, 458–466.
- 30 22 H. Liu, L. Zhang, X. Li, S. Huang, S. Liu, W. Xin, S. Xie, L. Xu, *J. Nat. Gas. Chem.*, 2009,  
31 **18**, 331–336.
- 32 23 D. Hua, S. Chen, G. Yuan, Y. Wang, L. Zhang, *Trans. Met. Chem.*, 2011, **36**, 245–248.
- 33 24 E. Mazoyer, K. Szeto, N. Merle, J. Thivolle-Cazat, O. Boyron, J. Basset, C. Nicholas, M.  
34 Taoufik, *J. Mol. Catal. A*, 2014, **385**, 125–132.
- 35 25 D. Hua, S. Chen, G. Yuan, Y. Wang, Q. Zhao, X. Wang, B. Fu, *Microporous & Mesoporous*  
36 *Mater.*, 2011, **143**, 320–325.
- 37 26 J. Hu, Y. Wang, L. Chen, R. Richards, W. Yang, Z. Liu, W. Xu, *Microporous &*  
38 *Mesoporous Mater.*, 2006, **93**, 158–163.
- 39 27 T. Bhuiyan, P. Arudra, M. Akhtar, A. Aitani, R. Abudawoud, M. Al-Yami, S. Al-Khattaf,  
40 *Appl. Catal. A*, 2013, **467**, 224–234.
- 41 28 A. Pamanathan, R. Maheswari, B. Grady, D. Moore, D. Barich, B. Subramaniam,  
42 *Microporous & Mesoporous Mater.*, 2013, **175**, 43–49.
- 43 29 B. Hu, H. Liu, K. Tao, C. Xiong, S. Zhou, *J. Phys. Chem. C*, 2013, **117**, 26385–26395.
- 44 30 W. Li, D. Y. Zhao, *Chem. Commun.*, 2013, **49**, 943–946.

- 1 31 J. Fan, C. Yu, F. Gao, J. Lei, B. Tian, L. Wang, Q. Luo, B. Tu, W. Zhou, D. Zhao, *Angew. Chem. Int. Ed.*, 2003, **42**, 3146–3150.
- 2
- 3 32 J. Liu, G. Lan, J. Peng, Y. Li, C. Li, Q. Yang, *Chem. Commun.*, 2013, **49**, 9558–9560.
- 4 33 L. Cao, M. Kruk, *RSC Adv.*, 2014, **4**, 331–339.
- 5 34 S. Huang, S. Liu, W. Xin, J. Bai, S. Xie, Q. Wang, L. Xu, *J. Mol. Catal. A.*, 2005, **226**, 61–68.
- 6
- 7 35 M. Kruk, C. Hui, *J. Am. Chem. Soc.*, 2008, **130**, 1528–1529.
- 8 36 S. Doniach, M. Sunjic, *J. Phys. C: Solid State Phys.*, 1970, **3**, 285–291.
- 9 37 S. Jeon, K. Yong, *J. Mater. Res.*, 2008, **23**, 1320–1326.
- 10 38 X. Yang, W. Dai, R. Gao, K. Fan, *J. Catal.*, 2007, **249**, 278–288.
- 11 39 X. Yang, R. Gao, W. Dai, K. Fan, *J. Phys. Chem. C*, 2008, **112**, 3819–3826.
- 12 40 D. Zhao, J. Feng, Q. Huo, N. Melosh, G. Fredrichson, B. Chmelka, G. Stucky, *Science*, 1998, **279**, 548–552.
- 13
- 14 41 J. Matos, M. Kruk, L. Mercuri, M. Jaroniec, L. Zhao, T. Kamiyama, O. Terasaki, T. Pinnavaia, Y. Liu, *J. Am. Chem. Soc.*, 2003, **125**, 821–829.
- 15
- 16 42 F. Kleitz, D. Liu, G. Anilkumar, I. Park, L. Solovyov, A. Shmakov, R. Ryoo, *J. Phys. Chem. B*, 2003, **107**, 14296–14300.
- 17
- 18 43 J. Fan, C. Yu, J. Lei, Q. Zhang, T. Li, B. Tu, W. Zhou, D. Zhao, *J. Am. Chem. Soc.*, 2005, **127**, 10794–10795.
- 19
- 20 44 Z. Zhang, J. Suo, X. Zhang, S. Li, *Appl. Catal. A*, 1999, **179**, 11–19.
- 21 45 S. Chaemchuen, S. Phatanasri, F. Verpoort, N. Sea-ma, K. Suriye, *Kinet. Catal.*, 2012, **53**, 247–252.
- 22
- 23
- 24
- 25
- 26
- 27
- 28
- 29
- 30
- 31
- 32
- 33

1

2

3

4

5

6 **Table 1. Binding energies, molar percentages of W<sup>6+</sup> and W<sup>5+</sup> species and WO<sub>3</sub>**  
 7 **crystalline sizes in different catalysts.**

Catalysts	Binding energies of W <sub>4f</sub> (eV)				W <sup>5+</sup> (%)	W <sup>6+</sup> (%)	The size of WO <sub>3</sub> (nm)
	W <sup>6+</sup> 4f <sub>5/2</sub>	W <sup>6+</sup> 4f <sub>7/2</sub>	W <sup>5+</sup> 4f <sub>5/2</sub>	W <sup>5+</sup> 4f <sub>7/2</sub>			
W-FDU-12-4.0%	38.4	36.3	37.1	35.0	80.9	19.1	N/A
WO <sub>3</sub> /FDU-12-4.0%	38.3	36.2	N/A	N/A	0	100	34
WO <sub>3</sub> /SiO <sub>2</sub> -4.0%	38.3	36.3	N/A	N/A	0	100	79
W-FDU-12-4.0%-700(cal)	38.2	36.2	N/A	N/A	0	100	--

8

9 **Table 2. BET surface areas, pore volumes, and pore sizes of FDU-12 and W-contained**  
 10 **materials.**

catalysts	BET surface area (m <sup>2</sup> /g)	Pore volume (cm <sup>3</sup> /g)	Pore size (nm)
FDU-12	717	0.70	17.6
W- FDU-12-1.2%	631	0.60	18.2
W- FDU-12-2.2%	624	0.61	18.5
W- FDU-12-3.0%	584	0.57	17.6
W- FDU-12-4.0%	582	0.60	17.4
W- FDU-12-5.2%	549	0.62	17.7

11

## 1 Figure captions

2 **Scheme 1.** Schematic diagram of the synthesis of doped mesoporous W-FDU-12.

3 **Figure 1.** TEM images of (a) FDU-12; (b) W-FDU-12-1.2%; (c) W-FDU- 12-3.0%; (d)  
4 W-FDU-12-4.0%; (e) W-FDU-12-5.2%; (f) W-FDU-4.0%-700(cal); (g)  
5 WO<sub>3</sub>/FDU-12-4.0%; and (h) WO<sub>3</sub>/SiO<sub>2</sub>-4.0% catalysts.

6 **Figure 2.** XPS spectra of (a) W-FDU-12-4.0%; (b) WO<sub>3</sub>/FDU-12-4.0%; (c) WO<sub>3</sub>/SiO<sub>2</sub>-4.0%;  
7 and (d) W-FDU-12-4.0%-700(cal) catalysts.

8 **Figure 3.** N<sub>2</sub> adsorption-desorption isotherms (left panel) and pore size distributions (right  
9 panel) showing (a) FDU-12; (b) W-FDU-12-1.2%; (c) W-FDU- 12-2.2%; (d)  
10 W-FDU-12-3.0%; (e) W-FDU-12-4.0%; and (f) W-FDU-12-5.2%.

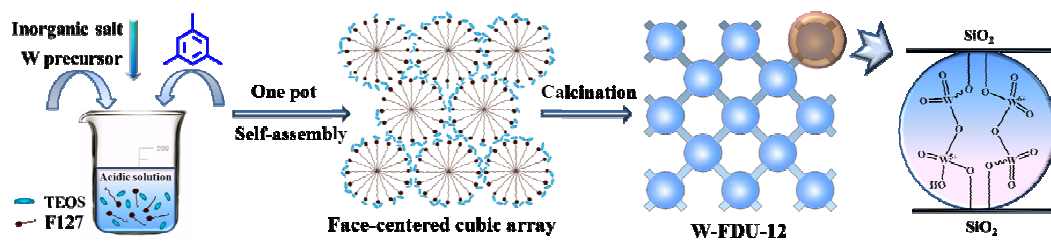
11 **Figure 4.** SAXS patterns of (a) FDU-12; (b) W-FDU-12-1.2%; (c) W-FDU- 12-2.2%; (d)  
12 W-FDU-12-3.0%; (e) W-FDU-12-4.0%; and (f) W-FDU-12-5.2% catalysts.

13 **Figure 5.** Wide-angle XRD profiles of different W containing materials showing (a) FDU-12;  
14 (b) W-FDU-12-1.2%; (c) W-FDU-12-2.2%; (d) W-FDU-12-3.0%; (e)  
15 W-FDU-12-4.0%; (f) W-FDU-12-5.2%; (g) WO<sub>3</sub>/FDU-12-4.0%; and (h)  
16 WO<sub>3</sub>/SiO<sub>2</sub>-4.0%.

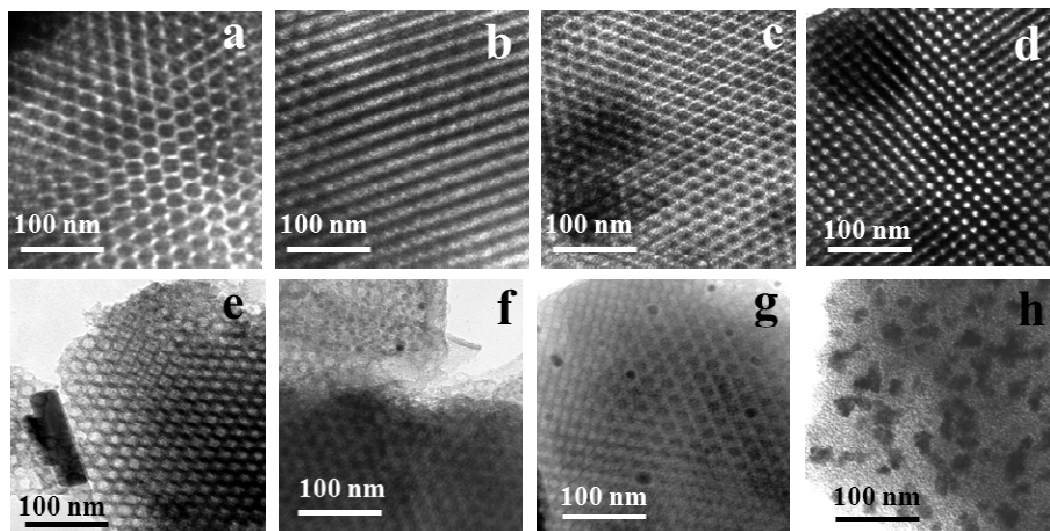
17 **Figure 6:** FTIR spectra of various samples showing (a) FDU-12; (b) W-FDU-12-1.2%; (c)  
18 W-FDU-12-2.2%; (d) W-FDU-12-3.0%; (e) W-FDU-12-4.0%; and (f)  
19 W-FDU-12-5.2%.

20 **Figure 7.** 1-Butene conversion (left panel) and propene selectivity (right panel) over  
21 W-FDU-12 catalysts with different W loadings. Reaction conditions: T=450 °C;  
22 P=0.1MPa; 1-C<sub>4</sub>H<sub>8</sub>/C<sub>2</sub>H<sub>4</sub>=1/2; WHSV (1-C<sub>4</sub>H<sub>8</sub>+C<sub>2</sub>H<sub>4</sub>) of 0.9 h<sup>-1</sup>; W-contained catalyst  
23 = 1.0 g.

24 **Figure 8.** 1-Butene conversion (left panel) and propene selectivity (right panel) over different  
25 4.0 wt% W-contained catalysts. Reaction conditions: T=450 °C; P=0.1 MPa;  
26 1-C<sub>4</sub>H<sub>8</sub>/C<sub>2</sub>H<sub>4</sub>=1/2; WHSV (1-C<sub>4</sub>H<sub>8</sub>+C<sub>2</sub>H<sub>4</sub>) of 0.9 h<sup>-1</sup>; W-contained catalyst=1.0 g.  
27

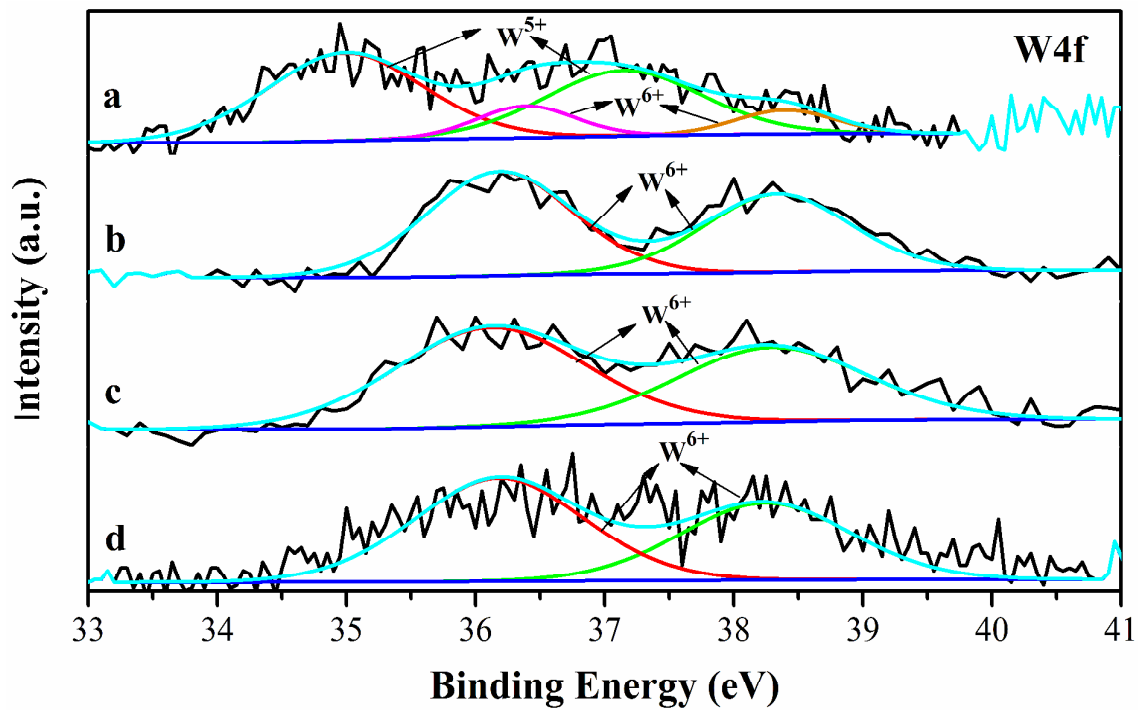


Scheme 1



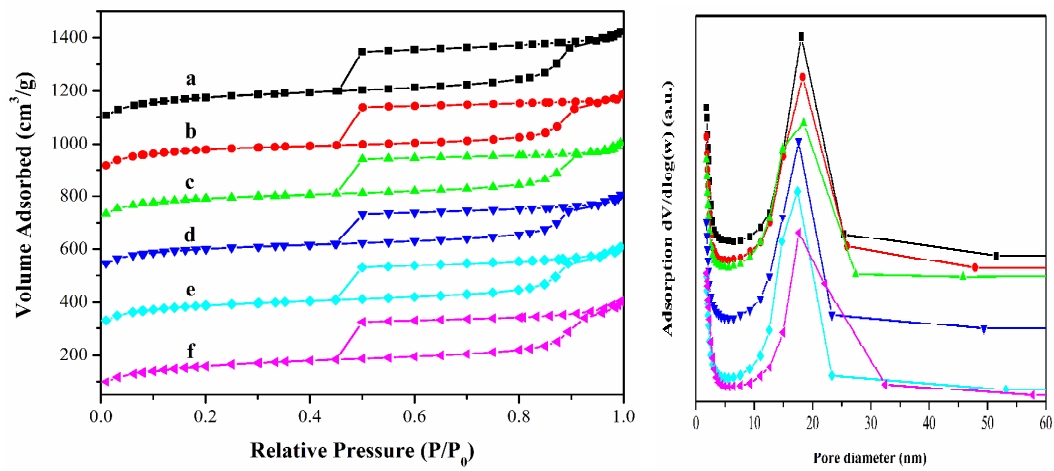
1

Figure 1



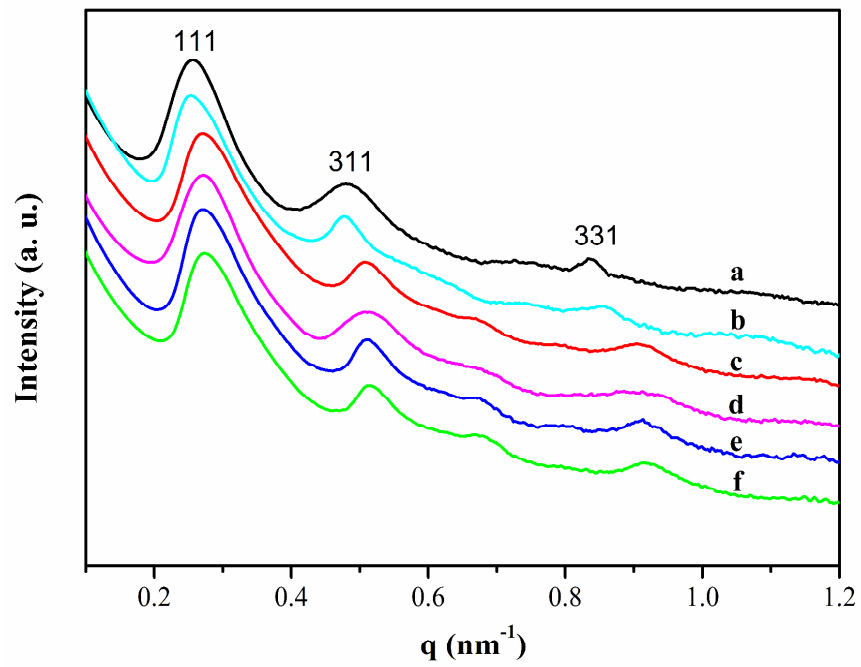
1

Figure 2



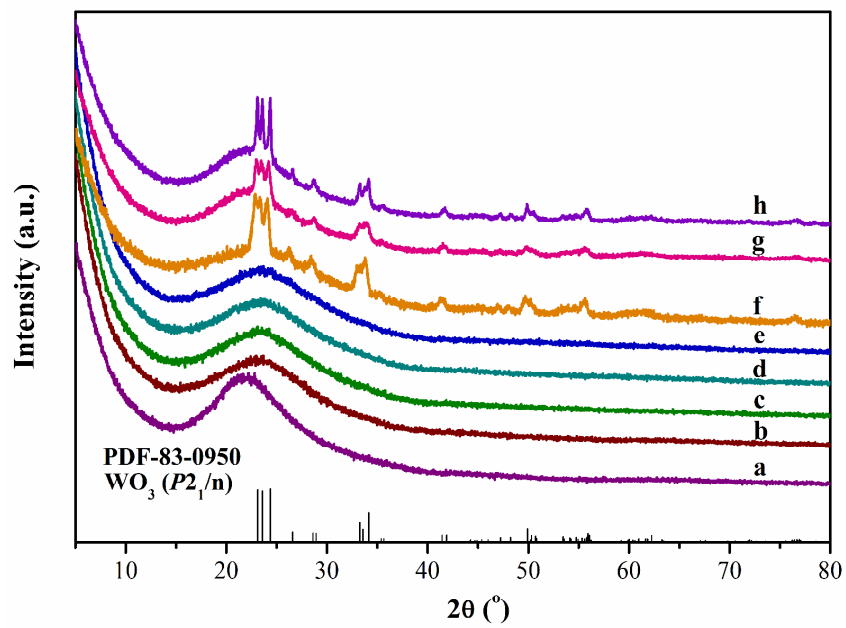
1

Figure 3



1

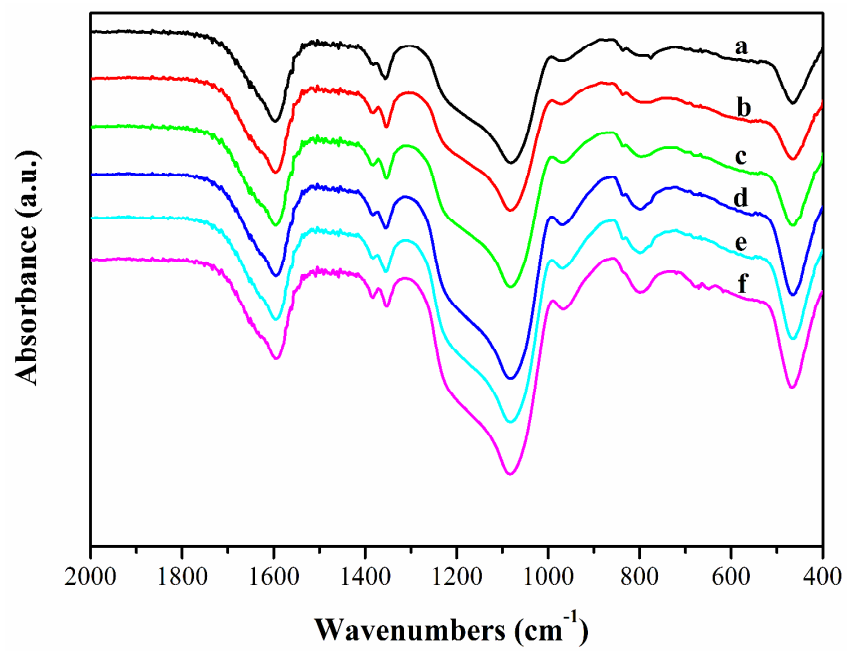
Figure 4



1

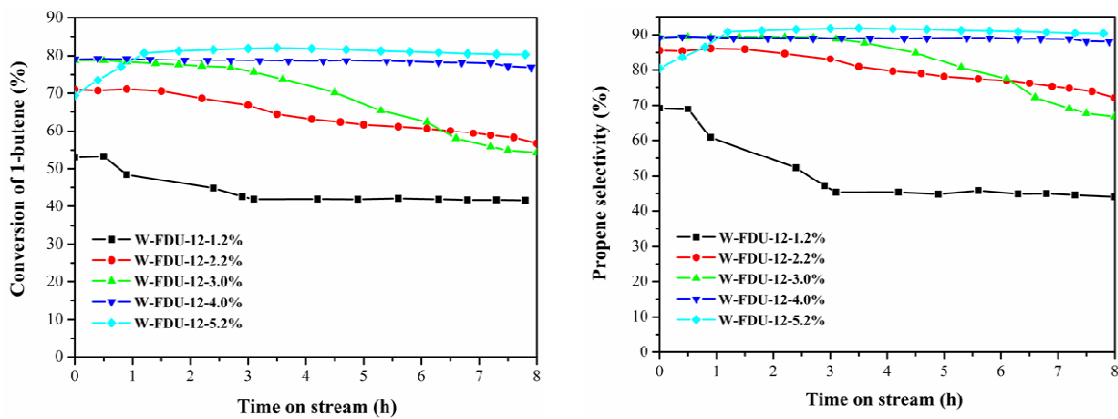
2

Figure 5



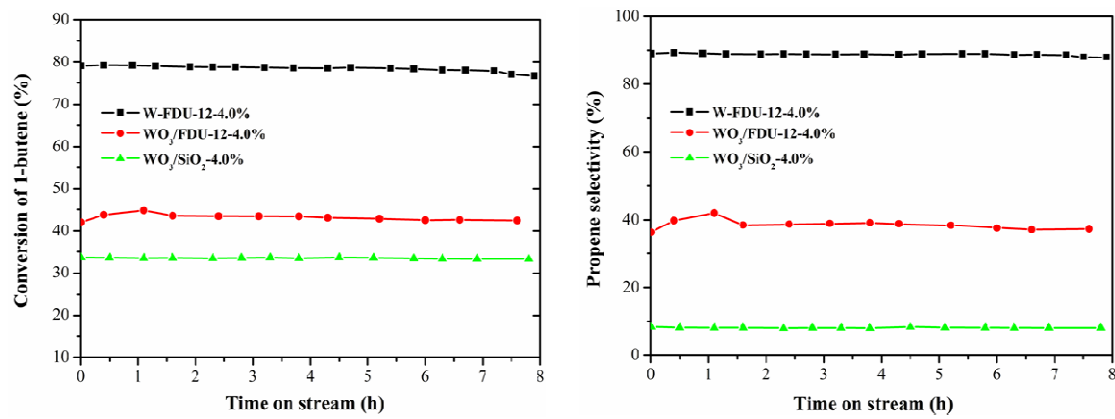
1

**Figure 6**



1

Figure 7



1

2

Figure 8